

Measurement of the $D^{*\pm}$ Meson Production Cross Section and $F_2^{c\bar{c}}$ at High Q^2 in ep Scattering at HERA

H1 Collaboration

Abstract

The inclusive production of $D^{*\pm}$ mesons in deep-inelastic $e^\pm p$ scattering is measured in the kinematic region of photon virtuality $100 < Q^2 < 1000 \text{ GeV}^2$ and inelasticity $0.02 < y < 0.7$. Single and double differential cross sections for inclusive D^* meson production are measured in the visible range defined by $|\eta(D^*)| < 1.5$ and $p_T(D^*) > 1.5 \text{ GeV}$. The data were collected by the H1 experiment during the period from 2004 to 2007 and correspond to an integrated luminosity of 351 pb^{-1} . The charm contribution, $F_2^{c\bar{c}}$, to the proton structure function F_2 is determined. The measurements are compared with QCD predictions.

Submitted to *Phys. Lett. B*

Dedicated to the memory of our dear friend and colleague, Beate Naroska

F.D. Aaron^{5,49}, C. Alexa⁵, K. Alimujiang^{11,51}, V. Andreev²⁵, B. Antunovic¹¹, S. Backovic³⁰, A. Baghdasaryan³⁸, E. Barrelet²⁹, W. Bartel¹¹, K. Begzsuren³⁵, A. Belousov²⁵, J.C. Bizot²⁷, V. Boudry²⁸, I. Bozovic-Jelisavcic², J. Bracinik³, G. Brandt¹¹, M. Brinkmann^{12,51}, V. Brisson²⁷, D. Bruncko¹⁶, A. Bunyatyan^{13,38}, G. Buschhorn²⁶, L. Bystritskaya²⁴, A.J. Campbell¹¹, K.B. Cantun Avila²², K. Cerny³², V. Cerny^{16,47}, V. Chekelian²⁶, A. Cholewa¹¹, J.G. Contreras²², J.A. Coughlan⁶, G. Cozzika¹⁰, J. Cvach³¹, J.B. Dainton¹⁸, K. Daum^{37,43}, M. Deák¹¹, B. Delcourt²⁷, J. Delvax⁴, E.A. De Wolf⁴, C. Diaconu²¹, V. Dodonov¹³, A. Dossanov²⁶, A. Dubak^{30,46}, G. Eckerlin¹¹, V. Efremenko²⁴, S. Egli³⁶, A. Eliseev²⁵, E. Elsen¹¹, A. Falkiewicz⁷, L. Favart⁴, A. Fedotov²⁴, R. Felst¹¹, J. Feltesse^{10,48}, J. Ferencei¹⁶, D.-J. Fischer¹¹, M. Fleischer¹¹, A. Fomenko²⁵, E. Gabathuler¹⁸, J. Gayler¹¹, S. Ghazaryan¹¹, A. Glazov¹¹, I. Glushkov³⁹, L. Goerlich⁷, N. Gogitidze²⁵, M. Gouzevitch¹¹, C. Grab⁴⁰, T. Greenshaw¹⁸, B.R. Grell¹¹, G. Grindhammer²⁶, S. Habib¹², D. Haidt¹¹, C. Helebrant¹¹, R.C.W. Henderson¹⁷, E. Hennekemper¹⁵, H. Henschel³⁹, M. Herbst¹⁵, G. Herrera²³, M. Hildebrandt³⁶, K.H. Hiller³⁹, D. Hoffmann²¹, R. Horisberger³⁶, T. Hreus^{4,44}, M. Jacquet²⁷, X. Janssen⁴, L. Jönsson²⁰, A.W. Jung¹⁵, H. Jung¹¹, M. Kapichine⁹, J. Katzy¹¹, I.R. Kenyon³, C. Kiesling²⁶, M. Klein¹⁸, C. Kleinwort¹¹, T. Kluge¹⁸, A. Knutsson¹¹, R. Kogler²⁶, P. Kostka³⁹, M. Kraemer¹¹, K. Krastev¹¹, J. Kretschmar¹⁸, A. Kropivnitskaya²⁴, K. Krüger¹⁵, K. Kutak¹¹, M.P.J. Landon¹⁹, W. Lange³⁹, G. Laštovička-Medin³⁰, P. Laycock¹⁸, A. Lebedev²⁵, V. Lendermann¹⁵, S. Levonian¹¹, G. Li²⁷, K. Lipka^{11,51}, A. Liptaj²⁶, B. List¹², J. List¹¹, N. Loktionova²⁵, R. Lopez-Fernandez²³, V. Lubimov²⁴, A. Makankine⁹, E. Malinovski²⁵, P. Marage⁴, Ll. Marti¹¹, H.-U. Martyn¹, S.J. Maxfield¹⁸, A. Mehta¹⁸, A.B. Meyer¹¹, H. Meyer¹¹, H. Meyer³⁷, J. Meyer¹¹, S. Mikocki⁷, I. Milcewicz-Mika⁷, F. Moreau²⁸, A. Morozov⁹, J.V. Morris⁶, M.U. Mozer⁴, M. Mudrinic², K. Müller⁴¹, P. Murín^{16,44}, Th. Naumann³⁹, P.R. Newman³, C. Niebuhr¹¹, A. Nikiforov¹¹, D. Nikitin⁹, G. Nowak⁷, K. Nowak⁴¹, J.E. Olsson¹¹, S. Osman²⁰, D. Ozerov²⁴, P. Pahl¹¹, V. Palichik⁹, I. Panagoulas^{1,11,42}, M. Pandurovic², Th. Papadopoulou^{1,11,42}, C. Pascaud²⁷, G.D. Patel¹⁸, O. Pejchal³², E. Perez^{10,45}, A. Petrukhin²⁴, I. Picuric³⁰, S. Piec³⁹, D. Pitzl¹¹, R. Plačakyte¹¹, B. Pokorný³², R. Polifka³², B. Povh¹³, V. Radescu¹⁴, A.J. Rahmat¹⁸, N. Raicevic³⁰, A. Rapiareza²⁶, T. Ravdandorj³⁵, P. Reimer³¹, E. Rizvi¹⁹, P. Robmann⁴¹, B. Roland⁴, R. Roosen⁴, A. Rostovtsev²⁴, M. Rotaru⁵, J.E. Ruiz Tabasco²², S. Rusakov²⁵, D. Šálek³², D.P.C. Sankey⁶, M. Sauter¹⁴, E. Sauvan²¹, S. Schmitt¹¹, L. Schoeffel¹⁰, A. Schöning¹⁴, H.-C. Schultz-Coulon¹⁵, F. Sefkow¹¹, R.N. Shaw-West³, L.N. Shtarkov²⁵, S. Shushkevich²⁶, T. Sloan¹⁷, I. Smiljanic², Y. Soloviev²⁵, P. Sopicki⁷, D. South⁸, V. Spaskov⁹, A. Specka²⁸, Z. Staykova¹¹, M. Steder¹¹, B. Stella³³, G. Stoicea⁵, U. Straumann⁴¹, D. Sunar¹¹, T. Sykora⁴, V. Tchoulakov⁹, G. Thompson¹⁹, P.D. Thompson³, T. Toll¹², F. Tomasz¹⁶, T.H. Tran²⁷, D. Traynor¹⁹, T.N. Trinh²¹, P. Truöl⁴¹, I. Tsakov³⁴, B. Tseepeldorj^{35,50}, J. Turnau⁷, K. Urban¹⁵, A. Valkárová³², C. Vallée²¹, P. Van Mechelen⁴, A. Vargas Trevino¹¹, Y. Vazdik²⁵, S. Vinokurova¹¹, V. Volchinski³⁸, M. von den Driesch¹¹, D. Wegener⁸, Ch. Wissing¹¹, E. Wunsch¹¹, J. Žáček³², J. Zálešák³¹, Z. Zhang²⁷, A. Zhokin²⁴, T. Zimmermann⁴⁰, H. Zohrabyan³⁸, and F. Zomer²⁷

¹ *I. Physikalisches Institut der RWTH, Aachen, Germany*

² *Vinca Institute of Nuclear Sciences, Belgrade, Serbia*

³ *School of Physics and Astronomy, University of Birmingham, Birmingham, UK^b*

⁴ *Inter-University Institute for High Energies ULB-VUB, Brussels and Universiteit Antwerpen, Antwerpen, Belgium^c*

- ⁵ *National Institute for Physics and Nuclear Engineering (NIPNE) , Bucharest, Romania*
- ⁶ *Rutherford Appleton Laboratory, Chilton, Didcot, UK^b*
- ⁷ *Institute for Nuclear Physics, Cracow, Poland^d*
- ⁸ *Institut für Physik, TU Dortmund, Dortmund, Germany^a*
- ⁹ *Joint Institute for Nuclear Research, Dubna, Russia*
- ¹⁰ *CEA, DSM/Irfu, CE-Saclay, Gif-sur-Yvette, France*
- ¹¹ *DESY, Hamburg, Germany*
- ¹² *Institut für Experimentalphysik, Universität Hamburg, Hamburg, Germany^a*
- ¹³ *Max-Planck-Institut für Kernphysik, Heidelberg, Germany*
- ¹⁴ *Physikalisches Institut, Universität Heidelberg, Heidelberg, Germany^a*
- ¹⁵ *Kirchhoff-Institut für Physik, Universität Heidelberg, Heidelberg, Germany^a*
- ¹⁶ *Institute of Experimental Physics, Slovak Academy of Sciences, Košice, Slovak Republic^f*
- ¹⁷ *Department of Physics, University of Lancaster, Lancaster, UK^b*
- ¹⁸ *Department of Physics, University of Liverpool, Liverpool, UK^b*
- ¹⁹ *Queen Mary and Westfield College, London, UK^b*
- ²⁰ *Physics Department, University of Lund, Lund, Sweden^g*
- ²¹ *CPPM, CNRS/IN2P3 - Univ. Mediterranee, Marseille, France*
- ²² *Departamento de Fisica Aplicada, CINVESTAV, Mérida, Yucatán, Mexico^j*
- ²³ *Departamento de Fisica, CINVESTAV IPN, México City, Mexico^j*
- ²⁴ *Institute for Theoretical and Experimental Physics, Moscow, Russia^k*
- ²⁵ *Lebedev Physical Institute, Moscow, Russia^e*
- ²⁶ *Max-Planck-Institut für Physik, München, Germany*
- ²⁷ *LAL, University Paris-Sud, CNRS/IN2P3, Orsay, France*
- ²⁸ *LLR, Ecole Polytechnique, CNRS/IN2P3, Palaiseau, France*
- ²⁹ *LPNHE, Universités Paris VI and VII, CNRS/IN2P3, Paris, France*
- ³⁰ *Faculty of Science, University of Montenegro, Podgorica, Montenegro^e*
- ³¹ *Institute of Physics, Academy of Sciences of the Czech Republic, Praha, Czech Republic^h*
- ³² *Faculty of Mathematics and Physics, Charles University, Praha, Czech Republic^h*
- ³³ *Dipartimento di Fisica Università di Roma Tre and INFN Roma 3, Roma, Italy*
- ³⁴ *Institute for Nuclear Research and Nuclear Energy, Sofia, Bulgaria^e*
- ³⁵ *Institute of Physics and Technology of the Mongolian Academy of Sciences , Ulaanbaatar, Mongolia*
- ³⁶ *Paul Scherrer Institut, Villigen, Switzerland*
- ³⁷ *Fachbereich C, Universität Wuppertal, Wuppertal, Germany*
- ³⁸ *Yerevan Physics Institute, Yerevan, Armenia*
- ³⁹ *DESY, Zeuthen, Germany*
- ⁴⁰ *Institut für Teilchenphysik, ETH, Zürich, Switzerlandⁱ*
- ⁴¹ *Physik-Institut der Universität Zürich, Zürich, Switzerlandⁱ*
- ⁴² *Also at Physics Department, National Technical University, Zografou Campus, GR-15773 Athens, Greece*
- ⁴³ *Also at Rechenzentrum, Universität Wuppertal, Wuppertal, Germany*
- ⁴⁴ *Also at University of P.J. Šafárik, Košice, Slovak Republic*
- ⁴⁵ *Also at CERN, Geneva, Switzerland*
- ⁴⁶ *Also at Max-Planck-Institut für Physik, München, Germany*
- ⁴⁷ *Also at Comenius University, Bratislava, Slovak Republic*

⁴⁸ Also at DESY and University Hamburg, Helmholtz Humboldt Research Award

⁴⁹ Also at Faculty of Physics, University of Bucharest, Bucharest, Romania

⁵⁰ Also at Ulaanbaatar University, Ulaanbaatar, Mongolia

⁵¹ Supported by the Initiative and Networking Fund of the Helmholtz Association (HGF) under the contract VH-NG-401.

^a Supported by the Bundesministerium für Bildung und Forschung, FRG, under contract numbers 05H09GUF, 05H09VHC, 05H09VHF, 05H16PEA

^b Supported by the UK Science and Technology Facilities Council, and formerly by the UK Particle Physics and Astronomy Research Council

^c Supported by FNRS-FWO-Vlaanderen, IISN-IKW and IWT and by Interuniversity Attraction Poles Programme, Belgian Science Policy

^d Partially Supported by Polish Ministry of Science and Higher Education, grant PBS/DESY/70/2006

^e Supported by the Deutsche Forschungsgemeinschaft

^f Supported by VEGA SR grant no. 2/7062/27

^g Supported by the Swedish Natural Science Research Council

^h Supported by the Ministry of Education of the Czech Republic under the projects LC527, INGO-1P05LA259 and MSM0021620859

ⁱ Supported by the Swiss National Science Foundation

^j Supported by CONACYT, México, grant 48778-F

^k Russian Foundation for Basic Research (RFBR), grant no 1329.2008.2

^l This project is co-funded by the European Social Fund (75%) and National Resources (25%) - (EPEAEK II) - PYTHAGORAS II

1 Introduction

The measurement of the charm quark production cross section in deep inelastic scattering (DIS) at HERA is a powerful means of testing perturbative quantum chromodynamics (QCD). Within this framework, a significant contribution to charm production arises from the boson-gluon fusion process which is sensitive to the gluon density in the proton. With increasing photon virtuality, Q^2 , the charm contribution to the inclusive ep scattering cross section rises from a few to up to 20%. Therefore, the treatment of the effects related to the charm quark contribution, in particular the mass effects, in perturbative QCD calculations is an important issue in the determination of parton distribution functions (PDFs). Different schemes to incorporate these effects are available.

Previous measurements were performed by identifying charm quarks via D mesons [1, 2] or using variables which are sensitive to the lifetime of heavy flavour hadrons [3, 4]. This paper presents a measurement of the $D^{*\pm}$ meson production cross section in the range of large photon virtualities $100 < Q^2 < 1000 \text{ GeV}^2$. The data were collected with the H1 detector at HERA during the running period 2004 – 2007 when HERA operated with 27.6 GeV electrons¹ and 920 GeV protons colliding at a centre of mass energy of $\sqrt{s} = 319 \text{ GeV}$ and correspond to the integrated luminosity of 351 pb^{-1} . The measured cross sections are compared to QCD predictions providing an insight into the dynamics of $D^{*\pm}$ meson production at high Q^2 . The charm contribution, $F_2^{c\bar{c}}$, to the proton structure function F_2 is determined.

2 H1 Detector

A detailed description of the H1 detector can be found elsewhere [5]. In the following only detector components relevant to this analysis are discussed. A right handed coordinate system is employed with the origin at the position of the nominal interaction point that has its z -axis pointing in the proton beam, or forward, direction and $x(y)$ pointing in the horizontal (vertical) direction. The pseudorapidity is related to the polar angle θ by $\eta = -\ln \tan(\theta/2)$.

Charged particle tracks are reconstructed in the central tracking detector (CTD). It consists of two cylindrical central jet drift chambers (CJC) placed concentrically around the beam-line, complemented by the silicon vertex detector [6], inside a solenoid with a homogeneous magnetic field of 1.16 T. The CJs are separated by a drift chamber which improves the z -coordinate reconstruction. A multiwire proportional chamber mainly used for triggering [7] is situated inside the inner CJC. The CTD provides a particle momentum measurement over the polar angle $15^\circ < \theta < 165^\circ$. The trajectories of charged particles are measured with a transverse momentum resolution of $\sigma(p_T)/p_T \approx 0.002 p_T/\text{GeV} \oplus 0.015$. The interaction vertex is reconstructed from CTD tracks. The Liquid Argon (LAr) calorimeter [8] is used to measure the energy and direction of electrons, photons and hadrons. It covers the polar angle range $4^\circ < \theta < 154^\circ$ with full azimuthal acceptance. Electromagnetic shower energies are measured with a precision of $\sigma(E)/E = 12\%/\sqrt{E/\text{GeV}} \oplus 1\%$ and hadronic energies with

¹In this paper “electron” is used to denote both electron and positron.

$\sigma(E)/E = 50\%/\sqrt{E/\text{GeV}} \oplus 2\%$, as determined in test beam measurements [9]. In the backward region, energy measurements are provided by a lead/scintillating-fibre (SpaCal) calorimeter [10] covering the angular range $155^\circ < \theta < 178^\circ$. For electrons a relative energy resolution of $\sigma(E)/E = 7\%/\sqrt{E/\text{GeV}} \oplus 1\%$ is reached, as determined in test beam measurements [11]. The SpaCal also provides time-of-flight information for trigger purposes. The luminosity is determined from the rate of the Bethe-Heitler reaction $ep \rightarrow ep\gamma$, measured using a photon detector located close to the beam pipe at $z = -103$ m, in the backward direction.

3 Models of Open Charm Production

Open charm production in electron-proton collisions can be described within different schemes. At energy scales larger than the charm quark mass, calculations can be performed within the zero-mass variable-flavour-number scheme (ZMVFNS) [12], where the charm quark is treated as a massless parton in the proton. The fixed-flavour-number scheme (FFNS) [13] applies close to the charm production threshold and takes into account heavy quark mass effects. In the latter scheme all quark flavours lighter than charm are treated as massless with massive charm being produced dynamically via boson-gluon fusion. A consistent treatment of heavy quarks in perturbative QCD over the full energy scale range should be provided through the generalised mass variable flavour number scheme (GMVFNS) [14].

The prediction of open charm production in FFNS at next-to-leading order (NLO) uses separate programs to calculate inclusive [13] and exclusive [15] (HVQDIS) quantities. The momentum densities of the three light quarks and the gluon in the proton are evolved using the DGLAP equations [16]. For the proton structure the FFNS PDF set MRST2004FF3 [17] is used. The charm quark mass is fixed to $m_c = 1.43$ GeV in accordance with this PDF set. The renormalisation and factorisation scales are set to $\mu_r = \mu_f = \mu_0 \equiv \sqrt{Q^2 + 4m_c^2}$. The charm fragmentation fraction into $D^{*\pm}$ mesons is taken as $f(c \rightarrow D^*) = 23.8 \pm 0.8\%$ [18] from the combination of measurements in e^+e^- experiments.

In the ZMVFNS calculation at NLO [12] a charm mass of 1.6 GeV, renormalisation and factorisation scales of $\mu_r = \mu_f = \mu_0 = \sqrt{Q^2 + 4m_c^2}$ and the CTEQ6.6M [19] parton densities are used. The perturbative fragmentation function [20] is evolved to the chosen scale of the transverse $D^{*\pm}$ momentum in the photon-proton rest frame, $p_T^*(D^*)$.

Events containing charm quarks are generated using the Monte Carlo programs RAPGAP [21] and CASCADE [22] and are passed through a detailed simulation of the detector response to determine the acceptance and efficiency and to evaluate the systematic uncertainties associated with the measurements.

The RAPGAP program, based on collinear factorisation and DGLAP evolution, is used to generate events containing $c\bar{c}$ pairs via photon-gluon fusion. The leading order (LO) matrix element with massive charm quarks is used. Parton showers, based on the DGLAP evolution, model the higher order QCD effects. The charm quark mass is set to 1.43 GeV. The proton structure is described by the PDF set CTEQ6.5M [23] and the factorisation and renormalisation scales are set to $\mu_r = \mu_f = \mu_0 = \sqrt{Q^2 + p_T^2}$.

The CASCADE program is based on the k_T factorisation approach. This calculation of the photon-gluon fusion matrix element takes into account the charm quark mass as well as the virtuality and transverse momentum of the incoming gluon. Gluon radiation from the incoming gluon as well as parton showers from the outgoing charm and anti-charm quarks are implemented in a manner which includes angular ordering constraints. The gluon density of the proton is evolved according to the CCFM equations [24]. The charm quark mass and the renormalisation scale are set to $m_c = 1.5 \text{ GeV}$ and $\mu_r = \sqrt{Q^2 + p_T^2}$, respectively. The unintegrated gluon distribution is described by the parametrisation set A0 [25].

The kinematics of $D^{*\pm}$ production depend not only on the charm quark production but also on the $c \rightarrow D^{*\pm}$ fragmentation process. The charm fragmentation function has been measured at H1 [26] using inclusive $D^{*\pm}$ meson production. The Kartvelishvili fragmentation function [27], which is controlled by a single parameter α , is used. The parameter values corresponding to the programs used in the present analysis are shown in Table 1. They depend on the centre of mass energy squared of the hard process, \hat{s} . To obtain the visible $D^{*\pm}$ production cross sections in HVQDIS, charm quarks are fragmented independently in the photon-proton centre of mass frame into $D^{*\pm}$ mesons according to Kartvelishvili function. In the RAPGAP and CASCADE programs hadronisation is performed using the Lund String Model [28, 29]. The momentum fraction of the charm quark carried by the $D^{*\pm}$ meson is modelled according to the Bowler parameterisation [30]. The longitudinal part of the fragmentation function is reweighted to the Kartvelishvili function.

Model	$\hat{s} < 70 \text{ GeV}^2$	$\hat{s} > 70 \text{ GeV}^2$
HVQDIS	$\alpha = 6.0_{-1.3}^{+1.1}$	$\alpha = 3.3_{-0.4}^{+0.4}$
RAPGAP	$\alpha = 10.3_{-1.6}^{+1.9}$	$\alpha = 4.4_{-0.5}^{+0.6}$
CASCADE	$\alpha = 8.4_{-1.1}^{+1.4}$	$\alpha = 4.5_{-0.6}^{+0.6}$

Table 1: Parameter α of the Kartvelishvili fragmentation function as used in the analysis.

The contribution of beauty production is estimated using the HVQDIS calculation, with hadronisation corrections determined using RAPGAP. The PDF set MRST2004FF3 is used with $m_b = 4.3 \text{ GeV}$ and $\mu_r = \mu_f = \mu_0 \equiv \sqrt{Q^2 + 4m_b^2}$. The fraction of beauty quarks producing $D^{*\pm}$ mesons is taken as $f(b \rightarrow D^*) = 17.3 \pm 2.0\%$ [31].

4 Event Selection and Signal Extraction

DIS events are selected by requiring a compact electromagnetic cluster in either the LAr or SpaCal calorimeters, which is taken to be the energy deposit of the scattered electron. The cluster has to be associated to a track reconstructed in the CTD. The events are triggered by either a coincidence of a SpaCal cluster and a signal from the CJC, or by the presence of a LAr cluster and a signal from the proportional chambers. The hadronic final state (HFS) particles are reconstructed using a combination of tracks and calorimeter deposits in an energy flow algorithm [32] which avoids double-counting. The event kinematics including the photon

virtuality Q^2 , the Bjorken scaling variable x and the inelasticity variable y are reconstructed with the $e\Sigma$ method [33], which uses the scattered electron and the HFS. The measurement is performed in the kinematic region $100 < Q^2 < 1000 \text{ GeV}^2$ and $0.02 < y < 0.7$.

The $D^{*\pm}$ mesons from the decays $D^{*\pm}(2010) \rightarrow D^0(1865)\pi_{slow}^\pm \rightarrow (K^\mp\pi^\pm)\pi_{slow}^\pm$ are reconstructed using the tracks in the CTD. The branching ratio for this channel amounts to $B = 2.63 \pm 0.04\%$ [34]. The invariant mass of the $K\pi$ combination is required to satisfy $|m(K\pi) - m(D^0)| < 80 \text{ MeV}$ where $m(D^0) = 1864.84 \text{ MeV}$ [34]. The decay angle θ^* of the kaon in the rest frame of the D^0 is restricted to $\cos\theta^* > -0.7$, in order to reduce the background, which strongly increases towards $\cos(\theta^*) = -1$ as opposed to the D^0 , which decays isotropically. To further reduce the combinatorial background, a Q^2 -dependent cut on the $D^{*\pm}$ transverse momentum, $p_T(D^*)/\text{GeV} > (3 \cdot [\log(Q^2/\text{GeV}^2) - 2] + 2)$, is applied. This criterion accounts for the increasing transverse momentum of the hadronic final state with rising Q^2 .

The $D^{*\pm}$ candidates in the pseudorapidity range $|\eta(D^*)| < 1.5$ are selected using the mass difference method [35]. In Fig. 1(a) the distribution of the mass difference $\Delta m = m(K\pi\pi) - m(K\pi)$ is shown for the selected data sample. A clear peak is observed around the nominal mass difference of 145.4 MeV . Wrong charge $K^\pm\pi^\pm\pi^\mp$ combinations with $K^\pm\pi^\pm$ pairs in the accepted D^0 mass range are used to describe the combinatorial background.

The number of $D^{*\pm}$ mesons is determined in each analysis bin from a simultaneous fit to the signal and the background distributions. The Crystal Ball function [36] is used for the signal description and the Granet parametrisation [37] for the background. Several fit parameters in the single and double-differential distributions are fixed using the full data sample and the Monte Carlo predictions [38].

The cross section presented in this paper corresponds to the kinematic range summarised in Table 2. The $p_T(D^*)$ and $\eta(D^*)$ range is chosen to be the same as in previous H1 analyses [1] at lower Q^2 . The Monte Carlo simulation is used for the extrapolation down to $p_T(D^*) = 1.5 \text{ GeV}$. This extrapolation typically leads to a 15% increase in the cross section. With all the selection cuts, the average acceptance amounts to around 30%.

Photon virtuality Q^2	$100 < Q^2 < 1000 \text{ GeV}^2$
Inelasticity y	$0.02 < y < 0.7$
Pseudorapidity of $D^{*\pm}$	$-1.5 < \eta(D^*) < 1.5$
Transverse momentum of $D^{*\pm}$	$p_T(D^*) > 1.5 \text{ GeV}$

Table 2: Definition of the kinematic range of the present analysis.

The inclusive $D^{*\pm}$ production cross section is studied differentially in the kinematic variables Q^2 , x , $p_T(D^*)$, $\eta(D^*)$ and the $D^{*\pm}$ inelasticity $z(D^*)$, which corresponds to the fraction of the virtual photon momentum carried by the $D^{*\pm}$ meson. The $D^{*\pm}$ inelasticity is determined as $z(D^*) = P \cdot p_{D^*} / P \cdot q = (E - p_z)_{D^*} / 2yE_e$, where E_e is the energy of the incoming electron and P , q and p_{D^*} denote the four-momenta of the incoming proton, the exchanged photon and the $D^{*\pm}$ meson, respectively. The cross section for $D^{*\pm}$ meson production is calculated from the observed number of $D^{*\pm}$ candidates $N_{D^{*\pm}}$, according to:

$$\sigma_{\text{vis}}(e^+p \rightarrow e^+D^{*\pm}X) = \frac{N_{D^{*\pm}} \cdot (1 - r)}{\mathcal{L}_{\text{int}} \cdot B \cdot \epsilon \cdot (1 + \delta_{\text{rad}})}, \quad (1)$$

where ϵ is the reconstruction efficiency, r the contribution from reflections, \mathcal{L}_{int} the integrated luminosity, B the branching ratio and δ_{rad} denotes the radiative corrections.

The reconstruction efficiency accounts for the trigger efficiency and the detector acceptance and is determined using the Monte Carlo simulation. For this purpose charm DIS events are generated using both the RAPGAP and CASCADE programs and the average efficiency is used. For the efficiency determination, RAPGAP is reweighted in Q^2 and CASCADE is reweighted in $p_T(D^*)$ in order to optimise the data description. The kinematic distributions of the $D^{*\pm}$ candidates compared with the reweighted Monte Carlo predictions are shown in Fig. 1(b)-(d).

The contribution r of reflections in the D^0 mass window from D^0 decay channels other than that considered in this analysis is estimated using the Monte Carlo simulation. This contribution amounts to $r = (4.4 \pm 0.5)\%$ independently of the $D^{*\pm}$ transverse momentum. The radiative corrections δ_{rad} are determined using RAPGAP interfaced to HERACLES 4.1 [39] and amount to 3% on average. The photoproduction background estimated using data [38] is not subtracted, but does not exceed 2.7%. The fraction of $D^{*\pm}$ mesons originating from $b\bar{b}$ events is estimated as described in section 3. It amounts to 4% on average and is included by definition in the inclusive $D^{*\pm}$ cross section. However, for the extraction of $F_2^{c\bar{c}}$, the predicted contribution from $b\bar{b}$ production is subtracted from the data.

5 Systematic Uncertainties

The systematic uncertainties are estimated by varying the input parameters to the Monte Carlo simulations within the experimental precision at the reconstructed level or the range allowed by the theoretical models at the generator level. The following correlated uncertainties are taken into account:

- The uncertainty on the hadronic energy scale is propagated to the measurement by changing the hadronic energy by $\pm 2\%$ ($\pm 3\%$) for events where the scattered electron is detected in the LAr (SpaCal) calorimeter. The uncertainty due to the scattered electron measurement is estimated by varying the electron energy by $\pm 1\%$ and the polar angle by ± 3 mrad, respectively.
- The trigger efficiency, luminosity and $D^* \rightarrow K\pi\pi$ branching ratio are known with uncertainties of 1%, 3.2% and 1.5%, respectively. An uncertainty of 1.2% on the cross-section measurement arises due to the uncertainty on the photoproduction background.
- The uncertainty on the reconstruction efficiency is taken as half of the difference between the two simulations, RAPGAP and CASCADE. This also covers the uncertainty on the extrapolation to $p_T(D^*) = 1.5$ GeV. The uncertainty in the efficiency determination due to the charm fragmentation model is estimated by varying the Kartvelishvili parameter α within its error as described in section 3. The uncertainty due to the choice of PDFs is estimated by using the CTEQ6L(LO) [40] parton densities in RAPGAP and the A2 set [41] in CASCADE as alternatives.

The following uncorrelated systematic uncertainties are accounted for:

- The signal shape and the invariant mass resolutions of the data are not fully reproduced by the Monte Carlo simulation. The errors on the $D^{*\pm}$ signal extraction are determined by varying the fit parameters within their uncertainties. The fraction of events outside the D^0 mass window is determined using the Monte Carlo simulation. Half of this fraction is taken as a systematic error to account for the uncertainty on the D^0 mass resolution.
- An uncertainty of 0.5% is assigned to the contribution from reflections to account for a possible p_T dependence. The uncertainty of the QED radiative corrections is 1.5%.

The following uncertainties are treated as partly correlated: The charged particle reconstruction uncertainty of 2.17%, which translates to 6.5% per $D^{*\pm}$ and the uncertainty on the electron track-cluster matching of 2%. The above uncertainties are added in quadrature to derive the experimental systematic error.

The theoretical uncertainties on the HVQDIS prediction are estimated by varying the input parameters as follows. The charm mass is varied from 1.3 to 1.6 GeV. The factorisation and renormalisation scales $\mu_f = \mu_r$ are varied simultaneously from $0.5\mu_0$ to $2\mu_0$. The fragmentation parameter is varied within its error as described in section 3. The parton density set CTEQ5F3 [42] is used as an alternative to MRST2004FF3. The resulting uncertainties, together with the error on $f(c \rightarrow D^*)$, are added in quadrature and are correlated between the bins. The uncertainties on the ZMFVNS prediction [12] are estimated by variation of the renormalisation and factorisation scales simultaneously from $0.5\mu_0$ to $2\mu_0$.

6 $D^{*\pm}$ Production Cross Section

The total inclusive cross section for $D^{*\pm}$ production in the phase space covered in this analysis (Table 2) is measured to be:

$$\sigma_{vis}(e^+p \rightarrow e^+D^{*\pm}X) = 225 \pm 14(\text{stat.}) \pm 27(\text{syst.}) \text{ pb} .$$

The corresponding predictions from RAPGAP, CASCADE and HVQDIS amount to 322 pb, 279 pb, and 241^{+14}_{-15} pb, respectively, including the $b\bar{b}$ contribution. In Fig. 2 and Table 3 differential cross sections are presented as a function of the DIS kinematic variables x and Q^2 and as a function of the D^* variables $p_T(D^*)$, $\eta(D^*)$ and $z(D^*)$. The data are compared to the expectations from the HVQDIS calculation and from the RAPGAP and CASCADE Monte Carlo simulations. Neither Monte Carlo simulation describes the shape and normalisation of the $D^{*\pm}$ kinematic distributions well, in contrast to the measurement [1] at lower Q^2 . The HVQDIS calculation agrees with the data within the theoretical uncertainties.

In Fig. 3 and Table 4 the double differential cross sections are shown as a function of y for different bins in Q^2 . The data are compared to the expectations of the HVQDIS calculation as well as to the RAPGAP and CASCADE simulations. HVQDIS describes the data well. Except for the first (Q^2, y) bin, the same holds for CASCADE. RAPGAP significantly overestimates the visible cross section.

The data are also compared to the ZMVFNS prediction [12]. This calculation has an intrinsic limitation on the transverse $D^{*\pm}$ momentum in the photon-proton center of mass frame, namely $p_T^*(D^*) > 2 \text{ GeV}$. Therefore the same additional cut is applied to the data and the cross section is determined for the corresponding phase space. In Fig. 4 the $D^{*\pm}$ cross sections are shown as a function of $p_T^*(D^*)$, $p_T(D^*)$, $\eta(D^*)$ and Q^2 , together with the ZMVFNS and HVQDIS calculations. The ZMVFNS prediction fails to describe the data, while HVQDIS agrees well with the data.

7 Extraction of $F_2^{c\bar{c}}$

The charm contribution $F_2^{c\bar{c}}(x, Q^2)$ to the inclusive proton structure function F_2 is defined by the expression for the single photon exchange cross section for charm production:

$$\frac{d^2\sigma^{c\bar{c}}}{dx dQ^2} = \frac{2\pi\alpha_{em}^2}{Q^4 x} ([1 + (1 - y)^2] F_2^{c\bar{c}}(x, Q^2) - y^2 F_L^{c\bar{c}}(x, Q^2)) \quad , \quad (2)$$

where α_{em} is the electromagnetic coupling constant. Weak interaction effects are neglected.

The contribution from the structure function $F_L^{c\bar{c}}$ amounts to at most 3% [13] in the present phase space and is neglected. The visible inclusive $D^{*\pm}$ cross sections $\sigma_{\text{vis}}^{\text{exp}}(y, Q^2)$ in bins of y and Q^2 are converted to a bin centre corrected $F_2^{c\bar{c}}(\langle x \rangle, \langle Q^2 \rangle)$ in the framework of a particular model using the relation:

$$F_2^{c\bar{c}}(\langle x \rangle, \langle Q^2 \rangle) = \frac{\sigma_{\text{vis}}^{\text{exp}}(y, Q^2)}{\sigma_{\text{vis}}^{\text{theo}}(y, Q^2)} \cdot F_2^{c\bar{c} \text{ theo}}(\langle x \rangle, \langle Q^2 \rangle) \quad , \quad (3)$$

where $\sigma_{\text{vis}}^{\text{theo}}$ and $F_2^{c\bar{c} \text{ theo}}$ are the theoretical predictions from the model under consideration. As in previous publications [1, 2] the HVQDIS program and another program [13] are used to calculate these quantities at NLO. CASCADE is not used for an $F_2^{c\bar{c}}$ extraction since it does not agree with the data (Fig. 2).

The model uncertainties on the measurement of $F_2^{c\bar{c}}$ are estimated by varying the HVQDIS parameters as described in section 5. The variations are made simultaneously in the calculation of the visible $D^{*\pm}$ cross sections and in the prediction for $F_2^{c\bar{c}}$. The total model uncertainties amount to 1 – 7% and are dominated by the variation of the renormalisation and factorisation scales. The central values of $F_2^{c\bar{c}}$ with experimental and model uncertainties are summarised in Table 5. The fraction of the total $D^{*\pm}$ cross section in the visible phase space, as predicted by HVQDIS and given by $\frac{\sigma(y, Q^2)_{\text{vis}}^{\text{theo}}}{\sigma(y, Q^2)_{\text{tot}}^{\text{theo}}}$, is also quoted and varies between 0.4 and 0.7.

In Fig. 5 $F_2^{c\bar{c}}$ is shown as a function of x for different values of Q^2 . The $F_2^{c\bar{c}}$ values are consistent with those obtained in an inclusive track measurement using the H1 vertex detector information [3]. The expectation from the recent PDF fit to inclusive DIS data, H1 PDF2009 [44], tends to overestimate the data. In Fig. 5(b) the measurements are compared to the massive FFNS calculation at NLO [13] and NNLO [46] and to the GMVFNS predictions at NLO and NNLO [45, 46]. The FFNS predictions agree well with the data over the full kinematic region investigated. The expectations for $F_2^{c\bar{c}}$ from a global fit in the GMVFNS at NLO tend to overestimate the data. At NNLO the GMVFNS prediction agrees better with the data.

8 Conclusions

The cross section for $D^{*\pm}$ meson production is measured in the phase space $100 < Q^2 < 1000 \text{ GeV}^2$ and $0.02 < y < 0.7$. Single and double differential cross sections are compared to Monte Carlo simulations and the predictions of NLO calculations in massive and massless schemes. The data have a typical precision of 20%.

In the measured domain the RAPGAP and CASCADE simulations do not provide good a description of the $D^{*\pm}$ kinematics. The double-differential cross section $d^2\sigma/dy dQ^2$ is described well by CASCADE, while RAPGAP overestimates the cross section at high Q^2 . The NLO FFNS calculation HVQDIS agrees with the data well, while the calculation based on ZMVFNS fails to describe the data.

The charm contribution $F_2^{c\bar{c}}$ to the proton structure function F_2 is determined. HVQDIS is used for extrapolation of the visible $D^{*\pm}$ cross sections to the full phase space in $p_T(D^*)$ and $\eta(D^*)$. The model uncertainties are found to be small in the kinematic region studied. The data are compared to QCD predictions at NLO in the FFNS scheme and to the CASCADE implementation of the CCFM model as well as to the expectations from global fit analyses, using GMFVNS implementations at NLO and NNLO. Both FFNS and CASCADE describe the measurement well. The data indicate that the NLO FFNS provides the best description of D^* production and of $F_2^{c\bar{c}}$ in the kinematic region of the analysis.

Acknowledgements

We are grateful to the HERA machine group whose outstanding efforts have made this experiment possible. We thank the engineers and technicians for their work in constructing and maintaining the H1 detector, our funding agencies for financial support, the DESY technical staff for continual assistance and the DESY directorate for support and the hospitality which they extend to the non-DESY members of the collaboration. Furthermore we thank G. Kramer and C. Sandoval for fruitful discussions.

References

- [1] A. Aktas *et al.* [H1 Collaboration], Eur. Phys. J. **C51** (2007) 271 [hep-ex/0701023];
C. Adloff *et al.* [H1 Collaboration], Phys. Lett. **B528** (2001) 199 [hep-ex/0108039];
C. Adloff *et al.* [H1 Collaboration], Nucl. Phys. **B545** (1999) 21 [hep-ex/9812023];
C. Adloff *et al.* [H1 Collaboration], Z. Phys. **C72** (1996) 593 [hep-ex/9607012].
- [2] S. Chekanov *et al.* [ZEUS Collaboration], Eur. Phys. J. **C63** (2009) 171 [arXiv:0812.3775];
J. Breitweg *et al.* [ZEUS Collaboration], Eur. Phys. J. **C12** (2000) 35 [hep-ex/9908012];

- S. Chekanov *et al.* [ZEUS Collaboration], Phys. Rev. **D69** (2004) 012004 [hep-ex/0308068];
- J. Breitweg *et al.* [ZEUS Collaboration], Phys. Lett. **B407** (1997) 402.
- [3] F. D. Aaron *et al.* [H1 Collaboration], accepted for publication by Eur. Phys. J. **C**, DESY-09-096, arXiv:0907.2643;
- A. Aktas *et al.* [H1 Collaboration], Eur. Phys. J. **C45** (2006) 23 [hep-ex/0507081].
- [4] S. Chekanov *et al.* [ZEUS Collaboration], accepted for publication by Eur. Phys. J. **C**, arXiv:0904.3487.
- [5] I. Abt *et al.* [H1 Collaboration], Nucl. Instrum. Meth. **A386** (1997) 310;
- I. Abt *et al.* [H1 Collaboration], Nucl. Instrum. Meth. **A386** (1997) 348.
- [6] D. Pitzl *et al.* [H1 Collaboration], Nucl. Instrum. Meth. **A454** (2000) 334 [hep-ex/0002044];
- B. List, Nucl. Instrum. Meth. **A501** (2001) 49.
- [7] J. Becker *et al.*, Nucl. Instrum. Meth. **A586** (2008) 190.
- [8] B. Andrieu *et al.* [H1 Calorimeter Group], Nucl. Instrum. Meth. **A336** (1993) 460.
- [9] B. Andrieu *et al.* [H1 Calorimeter Group], Nucl. Instrum. Meth. **A344** (1994) 492;
- B. Andrieu *et al.* [H1 Calorimeter Group], Nucl. Instrum. Meth. **A350** (1994) 57.
- [10] R. D. Appuhn *et al.* [H1 SpaCal Group], Nucl. Instrum. Meth. **A386** (1997) 397.
- [11] T. Nicholls *et al.* [H1 SpaCal Group], Nucl. Instrum. Meth. **A374** (1996) 149.
- [12] G. Heinrich, B. A. Kniehl, Phys. Rev. **D70** (2004) 094035 [hep-ph/0409303];
- C. Sandoval, Proc. of XVII International Workshop on Deep-Inelastic Scattering (DIS 2009), Madrid, 2009 arXiv:0908.0824;
- C. Sandoval, Ph.D. Thesis in preparation, Univ. Hamburg (2009).
- [13] E. Laenen, S. Riemersma, J. Smith and W. L. van Neerven, Phys. Lett. **B291** (1992) 325;
- E. Laenen *et al.*, Nucl. Phys. **B392** (1993) 162;
- S. Riemersma, J. Smith, and W. L. van Neerven, Phys. Lett. **B347** (1995) 143.
- [14] R. S. Thorne and W. K. Tung, Proc. of the Workshop HERA and the LHC, DESY-PROC-2009-02 (2009) 332 ISBN 978-3-935702032-4 arXiv:0809.0714.
- [15] B. W. Harris and J. Smith, Phys. Rev. **D57** (1998) 2806;
- B. W. Harris and J. Smith, Nucl. Phys. **B452** (1995) 109;
- B. W. Harris and J. Smith, Phys. Lett. **B353** (1995) 535.

- [16] V. N. Gribov and L. N. Lipatov, Sov. J. Nucl. Phys. **15** (1972) 675 [Yad. Fiz. **15** (1972) 1218];
 V. N. Gribov and L. N. Lipatov, Sov. J. Nucl. Phys. **15** (1972) 438 [Yad. Fiz. **15** (1972) 781];
 L. N. Lipatov, Sov. J. Nucl. Phys. **20** (1975) 94 [Yad. Fiz. **20** (1974) 181];
 Y. L. Dokshitzer, Sov. Phys. JETP **46** (1977) 641 [Zh. Eksp. Teor. Fiz. **73** (1977) 1216];
 G. Altarelli and G. Parisi, Nucl. Phys. **B126** (1977) 298.
- [17] A. D. Martin, W. J. Stirling and R. S. Thorne, Phys. Lett. **B636** (2006) 259 [hep-ph/0603143].
- [18] L. Gladilin, hep-ex/9912064;
 S. Chekanov *et al.* [ZEUS Collaboration], Eur. Phys. J. **C44** (2005) 351 [hep-ex/0508019].
- [19] P. M. Nadolsky *et al.*, Phys. Rev. **D78** (2008) 013004 [arXiv:802.0007].
- [20] T. Kneesch, B. A. Kniehl, G. Kramer, I. Schienbein, Nucl. Phys. **B799** (2008) 34 [arXiv:0712.0481].
- [21] H. Jung, Comp. Phys. Commun. **86** (1995) 147.
- [22] H. Jung and G. P. Salam, Eur. Phys. J. **C19** (2001) 351 [hep-ph/0012143];
 H. Jung, Comp. Phys. Commun. **143 100** (2002) 143 [hep-ph/0109102].
- [23] W. K. Tung *et al.*, JHEP0702 (2007) 053 [hep-ph/0611254].
- [24] M. Ciafaloni, Nucl. Phys. **B296** (1988) 49;
 S. Catani, F. Fiorani and G. Marchesini, Phys. Lett. **B234** (1990) 339;
 S. Catani, F. Fiorani and G. Marchesini, Nucl. Phys. **B336** (1990) 18;
 G. Marchesini, Nucl. Phys. **B445** (1995) 49 [hep-ph/9412327].
- [25] H. Jung, Proc. of the XII International Workshop on Deep Inelastic Scattering (DIS 2004), Strbske Pleso, Slovakia, April 14-18 (2004) Eds. D. Bruncko, J. Ferencei and P. Strizenec, IEP SAS, Kosice, Vol. **1** 299 hep-ph/0411287.
- [26] A. Aaron *et al.* [H1 Collaboration], Eur. Phys. J. **C59** (2009) 589.
- [27] V. G. Kartvelishvili, A. K. Likhoded and V. A. Petrov, Phys. Lett. **B78** (1978) 615.
- [28] B. Anderson, G. Gustafson, and B. Söderberg, Z. Phys. **C20** (1983) 317.
- [29] T. Sjöstrand, Comp. Phys. Commun. **135** (2001) 328 [hep-ph/0010017];
 T. Sjöstrand, L. Lönnblad and S. Mrenna, hep-ph/0108264.
- [30] M. G. Bowler, Z. Phys. **C11** (1981) 169;
 D. A. Morris, Nucl. Phys. **B313** (1989) 634.

- [31] K. Ackerstaff *et al.* [OPAL Collaboration], Eur. Phys. J. **C1** (1998) 439 [hep-ex/9708021].
- [32] M. Peetz, “Search for deviations from the Standard Model in high transverse energy processes at the electron-proton collider HERA”, Ph.D. thesis, Univ. Lyon (2003), DESY-THESIS-2003-023 (available at http://www-h1.desy.de/publications/theses_list.html);
S. Hellwig, “Untersuchung der $D^* - \pi_{slow}$ Double Tagging Methode in Charmanalysen”, Dipl. thesis, Univ. Hamburg (2004) (available at http://www-h1.desy.de/publications/theses_list.html).
- [33] U. Bassler, G. Bernardi, Nucl. Instrum. Meth. **A361** (1995) 197 [hep-ex/9412004];
U. Bassler, G. Bernardi. Nucl. Instrum. Meth. **A426** (1999) 583 [hep-ex/9801017].
- [34] C. Amsler *et al.* [Particle Data Group], Phys. Lett. **B667** (2008) 1.
- [35] G. J. Feldman *et al.*, Phys. Rev. Lett. **38** (1977) 1313.
- [36] J. E. Gaiser, Ph. D. Thesis, Stanford University (1982).
- [37] P. Granet *et al.* [French-Soviet-Collaboration], Nucl. Phys. **B140** (1978) 389.
- [38] M. Brinkmann, Ph. D. Thesis in preparation, Univ. Hamburg (2009) (to be available at http://www-h1.desy.de/publications/theses_list.html).
- [39] A. Kwiatkowski, H. Spiesberger, and H.J. Möhring, Proc. of the Workshop on Physics at HERA (1991), DESY, Hamburg, Vol. **3** (1992) 1294;
A. Kwiatkowski, H. Spiesberger, and H.J. Möhring, Z. Phys. **C50** (1991) 165.
- [40] J. Pumplin *et al.*, JHEP0207 (2002) 012 [hep-ph/0201195].
- [41] M. Hansson and H. Jung, Proc. of the XII International Workshop on Deep Inelastic Scattering (DIS 2003), St. Petersburg, Russia, April 23-27 (2003) hep-ph/0309009.
- [42] H. L. Lai *et al.*, Eur. Phys. J. **C12** (2000) 375 [hep-ph/9903282].
- [43] W. K. Tung *et al.*, JHEP0702 (2007) 053 [hep-ph/0611254]
- [44] F. D. Aaron *et al.* [H1 Collaboration], accepted for publication by Eur. Phys. J. **C**, DESY-09-005, arXiv:0904.3513.
- [45] R. S. Thorne, Phys. Rev. **D73** (2006) 054019 [hep-ph/0601245];
A. D. Martin, W. J. Stirling, R. S. Thorne, G. Watt, arXiv:0901.0002.
- [46] S. Alekhin, J. Blümlein, S. Klein, S. Moch, arXiv:0908.3128;
S. Alekhin, J. Blümlein, S. Klein, S. Moch, arXiv:0811.1412.

$p_T(D^*)[\text{GeV}]$	$\frac{d\sigma}{dp_T}[\frac{\text{pb}}{\text{GeV}}]$	$\delta_{stat}[\%]$	$\delta_{unc}[\%]$	$\delta_{cor}[\%]$
1.5 \div 6.0	27.8	11.1	7.4	+9.2 -8.9
6.0 \div 9.5	17.8	9.1	8.3	+8.3 -8.4
9.5 \div 20	3.31	11.4	11.6	+8.1 -8.1
$\eta(D^*)$	$\frac{d\sigma}{d\eta}[\text{pb}]$	$\delta_{stat}[\%]$	$\delta_{unc}[\%]$	$\delta_{cor}[\%]$
-1.5 \div -0.6	51.5	12.0	7.5	+7.4 -7.4
-0.6 \div 0.7	94.9	8.4	8.5	+9.7 -9.6
0.7 \div 1.5	68.1	16.4	8.8	+8.0 -8.2
$z(D^*)$	$\frac{d\sigma}{dz}[\text{pb}]$	$\delta_{stat}[\%]$	$\delta_{unc}[\%]$	$\delta_{cor}[\%]$
0.0 \div 0.3	234	17.3	7.8	+8.9 -8.7
0.3 \div 0.6	328	8.4	8.3	+8.6 -8.7
0.6 \div 1.0	135	8.8	9.0	+14.5 -13.8
$\log(\frac{Q^2}{\text{GeV}^2})$	$\frac{d\sigma}{dQ^2}[\frac{\text{pb}}{\text{GeV}^2}]$	$\delta_{stat}[\%]$	$\delta_{unc}[\%]$	$\delta_{cor}[\%]$
2.0 \div 2.2	1.88	10.1	7.6	+8.6 -8.7
2.2 \div 2.4	0.767	10.0	8.2	+7.7 -7.6
2.4 \div 3.0	0.0572	15.7	9.6	+9.7 -9.7
$\log(x)$	$\frac{d\sigma}{dx}[\text{pb}]$	$\delta_{stat}[\%]$	$\delta_{unc}[\%]$	$\delta_{cor}[\%]$
-2.8 \div -2.4	24.8×10^3	13.2	7.6	+6.9 -7.2
-2.4 \div -2.0	16.0×10^3	9.5	8.0	+9.5 -9.1
-2.0 \div -1.2	1.29×10^3	12.3	9.2	+10.2 -10.2

Table 3: Single differential cross sections for $D^{*\pm}$ production in bins of Q^2 , x and the meson kinematics, $p_T(D^*)$, $\eta(D^*)$ and $z(D^*)$, as measured in the visible range defined in Table 2. The central values of the cross section are listed together with relative statistical (δ_{stat}), uncorrelated (δ_{uncor}) and correlated (δ_{cor}) systematic uncertainties.

$\log(\frac{Q^2}{\text{GeV}^2})$	y	$\frac{d^2\sigma}{dQ^2 dy}[\frac{\text{pb}}{\text{GeV}^2}]$	$\delta_{stat}[\%]$	$\delta_{uncorr}[\%]$	$\delta_{corr}[\%]$
2.0 \div 2.2	0.020 \div 0.350	3.39	13.7	7.6	+11.6 -10.8
2.0 \div 2.2	0.350 \div 0.700	2.11	14.8	7.6	+6.4 -6.7
2.2 \div 2.4	0.020 \div 0.300	1.61	13.3	8.2	+8.0 -7.9
2.2 \div 2.4	0.300 \div 0.700	0.810	15.0	8.2	+7.6 -7.4
2.4 \div 3.0	0.020 \div 0.275	0.0921	24.8	9.6	+10.5 -10.4
2.4 \div 3.0	0.275 \div 0.700	0.0803	20.2	9.6	+9.7 -9.7

Table 4: Double differential cross sections for $D^{*\pm}$ production in bins of Q^2 and y as measured in the visible range defined in Table 2. The central values of the cross section are listed together with relative statistical (δ_{stat}), uncorrelated (δ_{unc}) and correlated (δ_{cor}) systematic uncertainties.

$\langle Q^2 \rangle [\text{GeV}^2]$	$\langle x \rangle$	$F_2^{c\bar{c}}$	$\delta_{stat} [\%]$	$\delta_{unc} [\%]$	$\delta_{cor} [\%]$	$\delta_{model} [\%]$	$\frac{\sigma(y, Q^2)_{vis}^{theo}}{\sigma(y, Q^2)_{tot}^{theo}}$
120	0.00924	0.122	13.7	7.6	+11.6 -10.8	+3.2 -3.8	0.53
120	0.00241	0.322	14.8	7.6	+6.4 -6.7	+3.4 -4.8	0.63
200	0.01240	0.168	13.3	8.2	+8.0 -7.9	+3.8 -4.6	0.48
200	0.00432	0.251	15.0	8.2	+7.6 -7.4	+3.3 -3.5	0.67
400	0.02480	0.072	24.8	9.6	+10.5 -10.4	+6.5 -5.9	0.43
400	0.01030	0.136	20.2	9.6	+9.7 -9.7	+3.7 -3.8	0.71

Table 5: The measured values and relative errors for the charm contribution to the proton structure function $F_2^{c\bar{c}}$. Relative statistical, correlated and uncorrelated experimental systematic as well as model uncertainties are listed. The fractions of the total $D^{*\pm}$ cross section in the visible phase space as predicted by HVQDIS are also given.

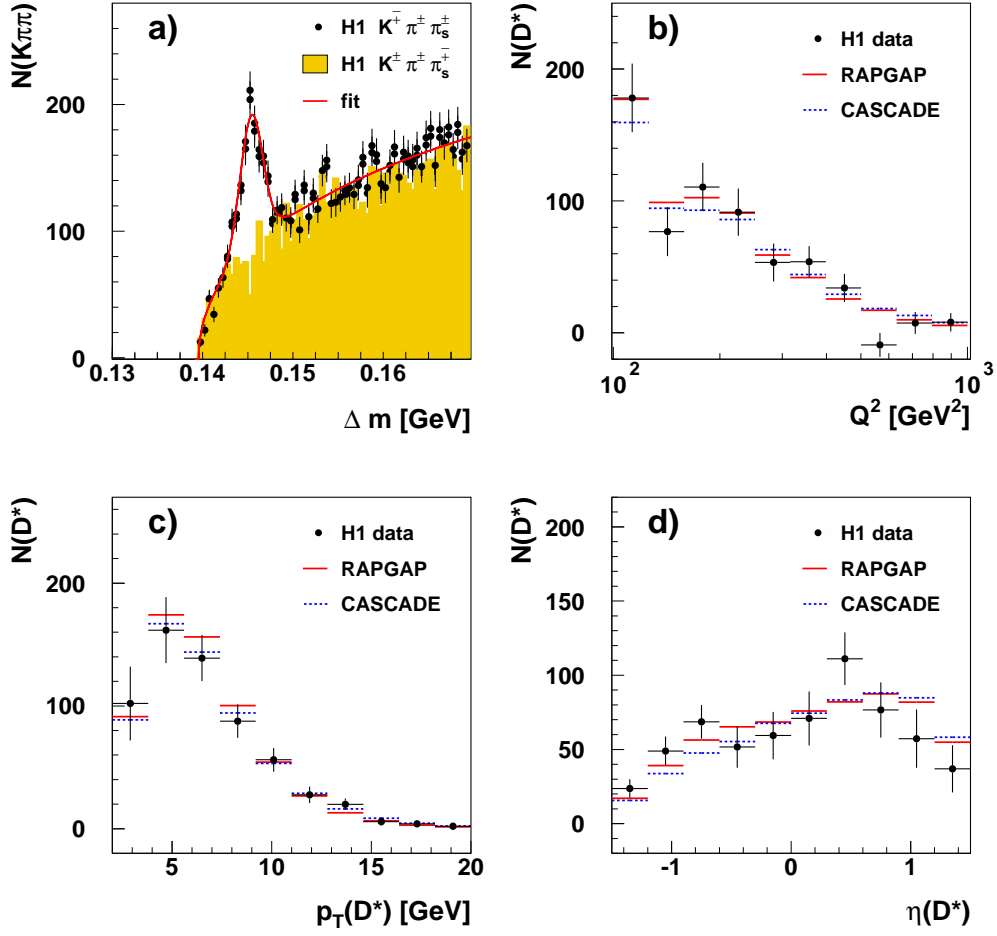


Figure 1: a) Distribution of $\Delta m = m(K\pi\pi) - m(K\pi)$ for $D^{*\pm}$ candidates ($K^{\mp}\pi^{\pm}\pi_s^{\pm}$) and for wrong charge combinations ($K^{\pm}\pi^{\pm}\pi_s^{\mp}$) in the accepted D^0 mass window. The fit function is also shown. Comparisons at the detector level between the $D^{*\pm}$ data sample and the reweighted Monte Carlo models are presented. Background-subtracted distributions are shown as a function of Q^2 (b), $p_T(D^*)$ (c) and $\eta(D^*)$ (d).

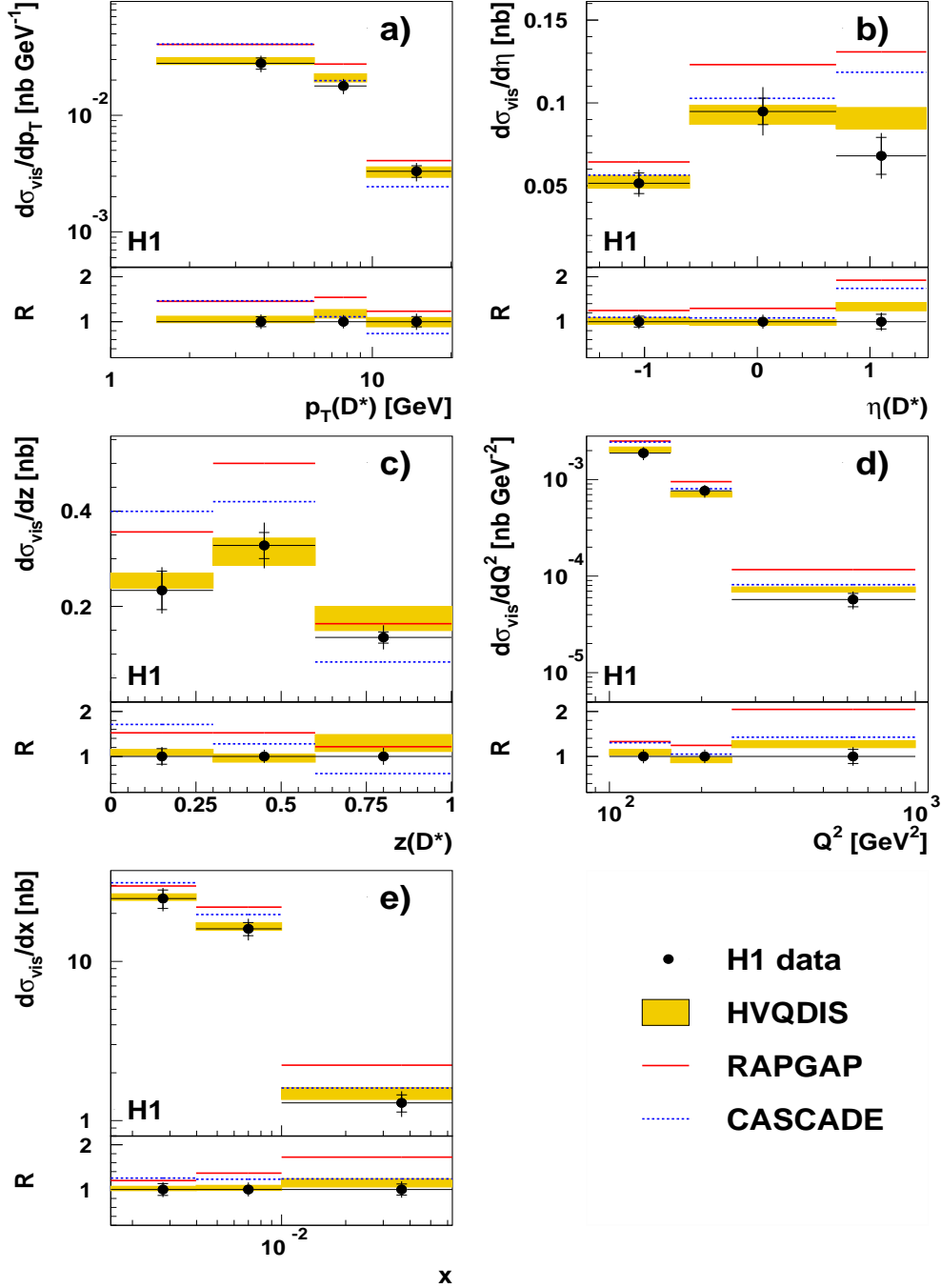


Figure 2: Differential cross sections for inclusive $D^{*\pm}$ meson production as a function of $p_T(D^*)$, $\eta(D^*)$, $z(D^*)$, Q^2 and x . The inner error bars indicate the statistical uncertainties, the outer error bars show the statistical and systematic uncertainties added in quadrature. The expectations of CASCADE (dashed line) and RAPGAP (solid line) are obtained using the parameters as described in section 3. The band of the HVQDIS prediction (shaded) is obtained using the parameter variation described in section 5. The ratio $R = \sigma_{theory}/\sigma_{data}$ is also shown. In the case of HVQDIS the theoretical uncertainties are taken into account. The inner error bars on the data points at $R = 1$ display the relative statistical errors, and the outer error bars show the relative statistical and systematic uncertainties added in quadrature.

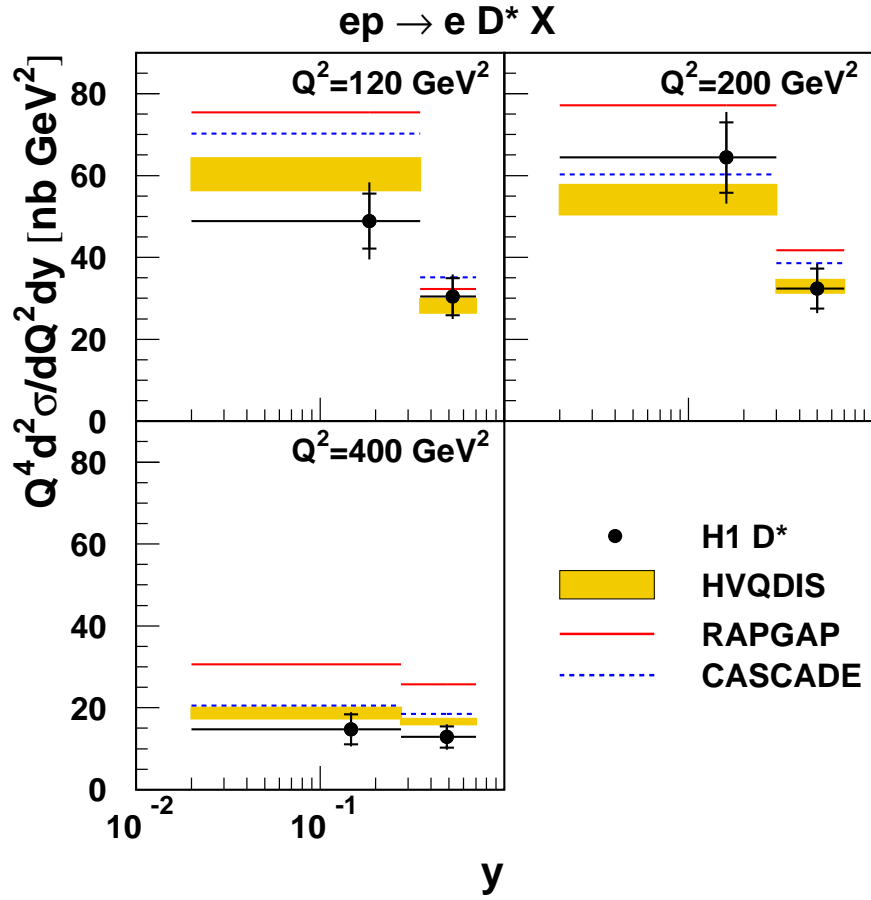


Figure 3: Double-differential cross sections for $D^{*\pm}$ production as a function of y in different Q^2 bins. For the purpose of presentation the cross sections are multiplied by Q^4 . The data (closed symbols) are shown with the statistical (inner error bars) and total (full error bars) uncertainties. Predictions from the RAPGAP (solid line) and CASCADE (dashed line) Monte Carlo simulations and the HVQDIS NLO calculation (shaded area) are also shown.

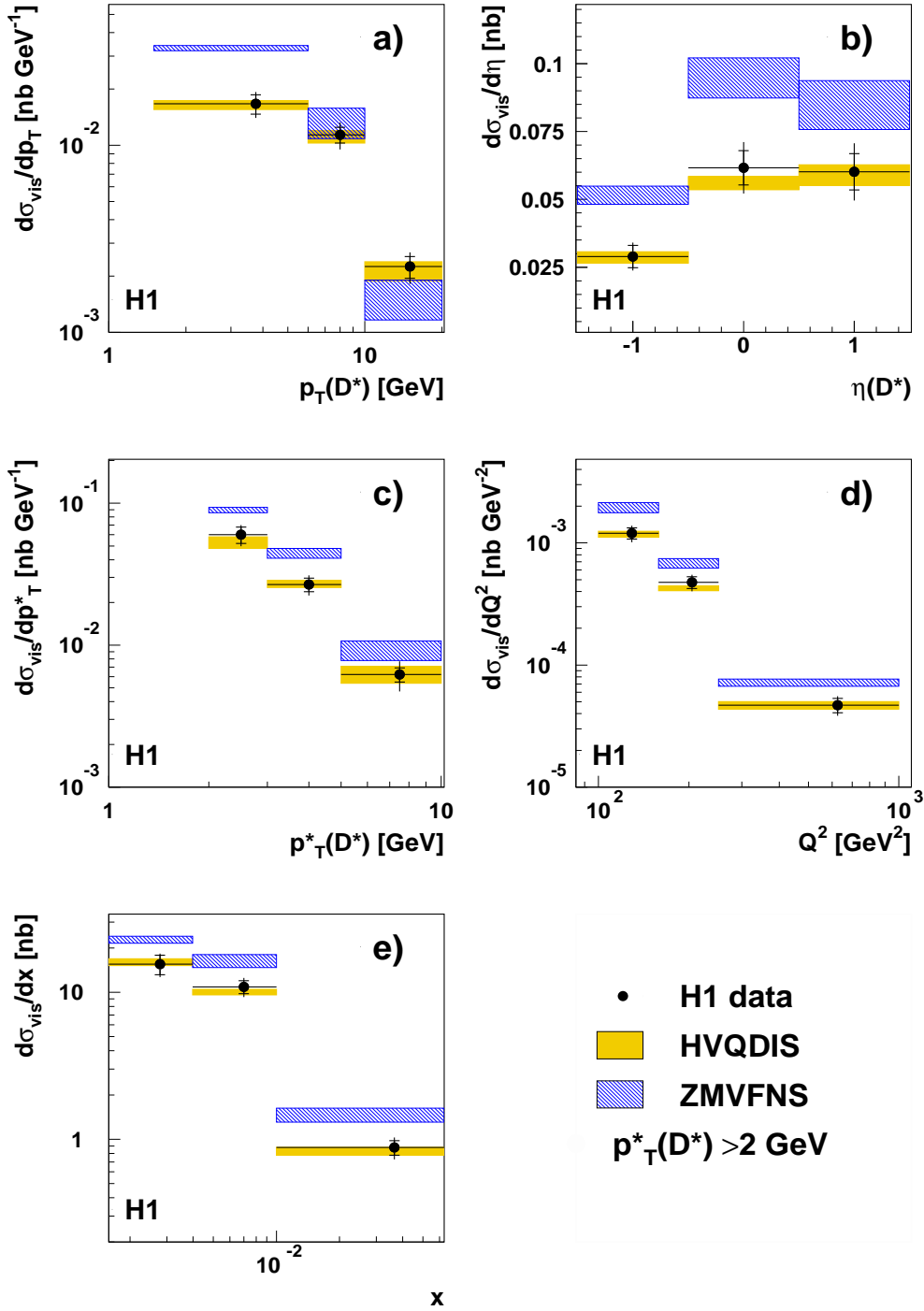


Figure 4: Differential cross sections for inclusive $D^{*\pm}$ meson production as a function of $p_T(D^*)$, $\eta(D^*)$, $p_T^*(D^*)$, Q^2 and x as measured for $p_T^*(D^*) > 2 \text{ GeV}$. The inner error bars indicate the statistical uncertainties, the outer error bars show the statistical and systematic uncertainties added in quadrature. The expectation of HVQDIS (shaded band) is obtained using the parameter variation described in section 5. The prediction in ZMVFNS is represented by the hatched band where the uncertainty originates from the scale variation.

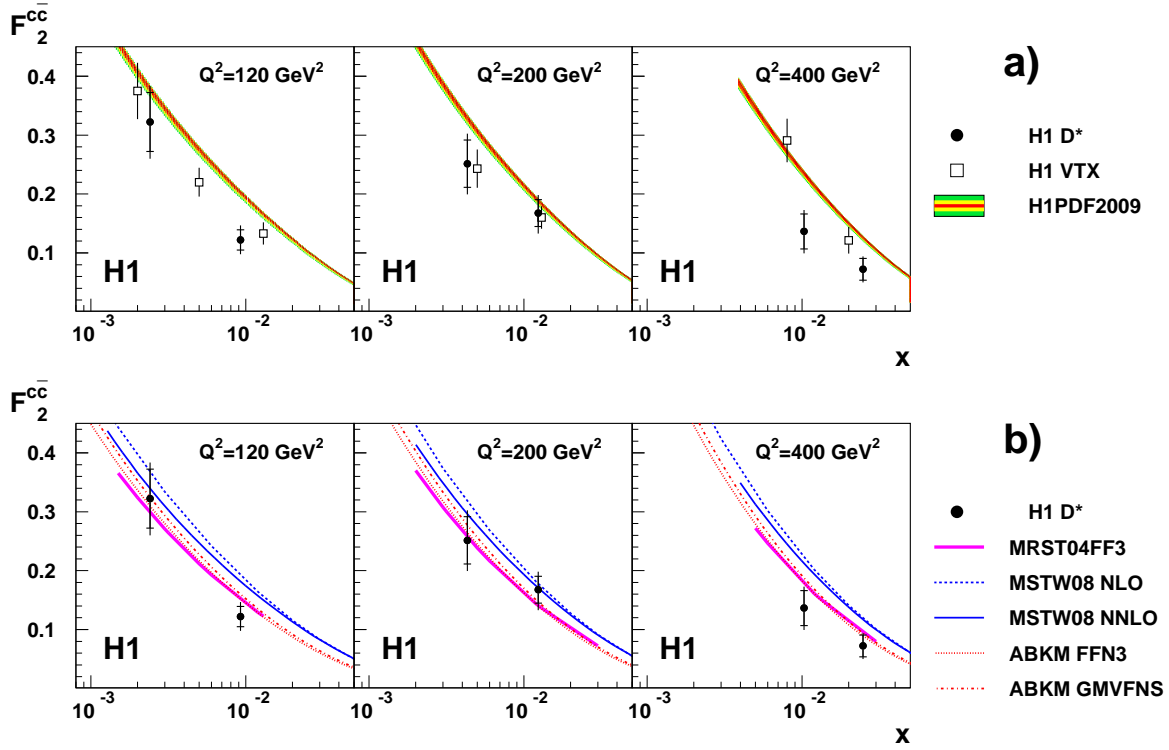


Figure 5: The charm contribution $F_2^{c\bar{c}}$ to the proton structure function. The data (closed symbols) are shown with statistical (inner error bars) and total (full error bars) uncertainties. In a) the data are compared to the H1 measurement of $F_2^{c\bar{c}}$ using secondary vertex information (open symbols) [3], where measurements at $Q^2 = 300 \text{ GeV}^2$ are shifted to $Q^2 = 400 \text{ GeV}^2$ using the NLO calculation [13]. The result of the PDF fit H1PDF2009 (shaded band) is also shown. The uncertainty band accounts for experimental, model and parametrisation uncertainties [44]. In b) the data are compared to the QCD predictions from the NLO calculation [13] in FFNS (light thick solid line). The predictions from the global PDF fits MSTW08 at NLO (dashed) and NNLO (dark solid) as well as the results of the ABKM fit [46] at NNLO in FFNS (dotted) and GMVFNS (dashed-dotted) are also shown.